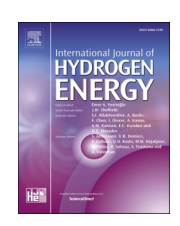
ELSEVIER

Contents lists available at ScienceDirect

International Journal of Hydrogen Energy

journal homepage: www.elsevier.com/locate/he





Liquid phase laser ablation as a general green physical etching method to prepare MXene dots with arbitrary surface functionalization. Implications in overall water splitting photocatalysis

Rubén Ramírez-Grau ^a ^b, María Cabrero-Antonino ^a ^b, Francis Rey Cortes ^b, Gladys Mínguez-Vega ^b ^b, Matthew G. Quesne ^c ^b, C. Richard A. Catlow ^{d,e} ^b, Jose A. Mata ^f ^b, Hermenegildo García ^{a,*} ^b, Ana Primo ^a ^b

ARTICLE INFO

Keywords: MXene dots Pulsed laser ablation Physical MAX etching MXene as photocatalysts

ABSTRACT

A novel green, fluoride-free etching method allowing installation of surface groups at will for the preparation 0D MXene dots with notable photocatalytic activity is reported. The method consists in the liquid-phase laser ablation using a pulsed Nd-YAG laser (532 nm, 7 ns fwhp, 30 mJ pulse $^{-1}$, 10 Hz) that produces the physical Al etching of the Ti₃AlC₂ precursor forming nanometric Ti₃C₂ particles. Simultaneously with etching, the surface of the MXene dots become functionalized with organic moieties inherited from the liquid phase as confirmed by XPS and in several cases by FT-IR spectroscopy. The lateral particle size of the Ti₃C₂ dots depends on the viscosity of the liquid medium and varies from a few nm to above 50 nm. Crystallinity and structure of the Ti₃C₂ dot is confirmed by high resolution TEM and by selected area electron diffraction of the samples. Ti₃C₂ dots promote photocatalytic overall water splitting into H₂ and O₂, the activity depending on the nature of the surface terminal groups. However, upon reuse the Ti₃C₂ dots become significantly degraded into amorphous material, decreasing gradually in photocatalytic activity. This degradation is proposed to be caused by self-oxidation of Ti₃C₂ dots by the photogenerated holes, as evidenced by the fact that the use of methanol as hole quencher stops deactivation during H₂ production. In sharp contrast with the decay in photocatalytic activity the presence of hole quenchers, the Ti₃C₂ dots even increase substantially their photocatalytic activity upon reuse, a fact that has been attributed to the optimization of the nature of the surface terminal groups during the photocatalytic process.

1. Introduction

MXenes are becoming among the most researched 2D nanomaterials, since they offer considerable chemical diversity regarding the elements that can be included in their composition, as well as unique physical properties such as electrical conductivity, microwave shielding and electrocatalytic activity to name a few [1,2]. One of the main drawbacks that limit wider MXene application is the negative environmental impact regarding the use of HF and fluorinated salts in the etching process converting the MAX precursors into the MXene material [3].

While the use of fluorine containing agents can be avoided by alternative molten salt etching procedures [4], the large excess of the chloride salts, as well as Lewis acid metal ions, employed in the molten salt etching process still produce large amounts of aqueous wastes that require adequate treatment. Therefore, it will be highly convenient to develop general physical methods able to convert the MAX phase into the corresponding MXene without the need of chemicals, thus, avoiding or minimizing chemical wastes.

Besides, the environmental impact and safety issues related to chemical etching and the use of HF, another problem that still remains

E-mail address: hgarcia@qim.upv.es (H. García).

https://doi.org/10.1016/j.ijhydene.2025.152298

^a Instituto de Tecnología Química Universitat Politècnica de València-Consejo Superior de Investigaciones Científicas, Universitat Politècnica de Valencia, Av. De Los Naranjos S/n, 46022, Valencia, Spain

^b Group of Optics-UJI (GROC-UJI), Institute of New Imaging Technologies (INIT), Universitat Jaume I, 12071, Castellón, Spain

^c School of Chemistry, University of Leeds, UK

d Department of Chemistry, University College London, 20-Gordon Street, London, WC1 HOAJ, UK

e School of Chemistry, Cardiff University, Park Place, Cardiff, CF10 3AT, UK

f Institute of Advanced Materials (INAM), Universitat Jaume I, Avda. Sos Baynat S/n, 12006, Castellón, Spain

 $^{^{\}ast}$ Corresponding author.

unsolved in MXene synthesis is the control of the terminal groups installed on the surface of the MXene particles [5]. The nature of the surface groups depends on the etching reagent employed during MXene preparation and they cannot be selected at will during MXene synthesis. After the synthesis, modification of the surface groups requires additional post synthetic reactions that frequently lead to incomplete surface termination exchange and need extra workup besides to produce further chemical wastes [6]. It would be a significant breakthrough in the MXene area if simultaneously to a green MAX etching process the wanted surface termination could be introduced. This important advance could be possible if a physical etching method is carried out in the presence of a variety of nucleophilic agents that provide the surface termination. Surface terminal groups are crucial determining many properties of the resulting MXene sample, since they control collective properties of the material, such as the work function of the material and the electron density distribution [7,8].

A third advance in MXene materials will be the control of the lateral size down to tens of nanometers in which quantum confinement effects can operate [9]. Nanoparticles often exhibit unique properties derived from their small dimensions in comparison to larger micrometric particles [10]. Frequently the enhanced nanoparticle performance derives from the large surface-to-volume ratio that exposes a larger proportion of atoms at the surface and increases the density of defects with under coordinated atoms [11]. In addition, electron localization is a small space, like in quantum dots or plasmonic nanoparticles, can cause optoelectronic effects as consequence of confinement [9]. Particularly in highly conductive 2D nanomaterials, a decrease of their particle size can open a gap between the occupied and unoccupied electronic states, converting them into semiconductors [12].

The present study shows how these three parameters, i.e. i) etching in the absence of corrosive and hazardous chemicals, ii) flexibility in the installment of surface termination, and iii) control of the lateral dimension at the nano scale can be achieved by laser ablation of the MAX precursor in liquid phase suspension. To illustrate the advantage of nanometric 0 D MXene particles whose preparation is described here, we will show the photocatalytic activity of these MXene dots for overall water splitting into $\rm H_2$ and $\rm O_2$, reaching remarkable photocatalytic efficiency that depends on the nature of the surface terminal group. In view of the theoretical predictions is very likely that the nature of surface terminal groups has a similar influence on other processes.

2. Results and discussion

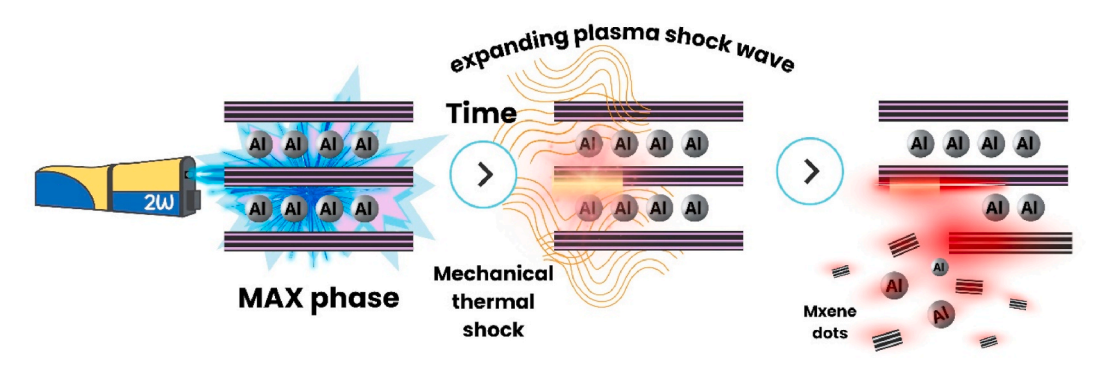
2.1. Ti₃C₂ sample preparation and characterization

The present study has focused on the most widely studied Ti_3C_2 MXene to illustrate the potential of laser ablation as a physical etching process of general applicability that besides avoiding the use of chemicals, can introduce arbitrarily at will surface terminations, depending on the compound present in the liquid medium during the process. Laser

ablation was carried out with a pulsed Nd – YAG laser operating at the second harmonic wavelength (532 nm) at a frequency of 10 pulse s⁻¹, with an average pulse energy of 30 mJ pulse⁻¹. In this physical etching procedure, the Ti₃AlC₂ precursor was placed in a 5 mL quartz cuvette containing a liquid medium. The cuvette was capped with a septum and purged for at least 15 min with Ar before starting the physical etching. After the liquid phase laser ablation, any remaining solid was decanted, obtaining a persistent suspension. The solvent can be removed under reduced pressure. In the specific cases of laser ablation in allyl and benzyl alcohols as solvents, occurrence of some oligo-/polymerization of these alcohols was evident from the higher mass of the residue. Scheme 1 presents an illustration of the process. Typical etching time was 10 h. Several alcohols were used as liquid media. Besides pure alcohols as solvents, a solution of tetrabutylammonium hydroxide (TBAOH) in ethanol was also used. TBAOH has been reported as an efficient exfoliating agent for multilayer Ti₃C₂ upon sonication, since it introduces surface -OH groups and TBA+ ions on the surface [13,14]. It was expected that the same reactivity could also happen here during the laser ablation, thereby possibly promoting exfoliation and increasing hydrophilicity. Table 1 indicates the samples prepared in the present study.

After laser ablation, the samples were characterized by TEM and by UV–Vis, IR and X-ray photoelectron spectroscopies. TEM images provided an important information about the structure of the resulting material, confirming in every case its crystallinity by observation of the characteristic atomic fringe spacing corresponding to ${\rm Ti}_3{\rm C}_2$ MXenes and by the pattern in the selected area electron diffraction of the samples. Fig. 1 shows selected images, while Fig. S1 in supporting information contains additional TEM images for the other ${\rm Ti}_3{\rm C}_2$ of the series. Minor variations in the fringe distance depending on the surface functionalization from 0.253 to 0.269 nm were observed (see Table 1) that probably reflect the structural stress caused by the bonding with the surface terminations and/or the influence of the particle thickness of the sample. Worth noting is that this spacing is characteristic of the ${\rm Ti}_3{\rm C}_2$ and similar to the (103) plane of the MAX ${\rm Ti}_3{\rm AlC}_2$ precursor (0.260 nm).

The average lateral particle size for the various Ti₃C₂ dots was determined by measuring the dimensions of a statistically relevant number of particles. In the cases of benzyl, and allyl alcohols, it was observed that the primary Ti₃C₂ particles agglomerate into larger aggregates trapped within an organic matrix. However, focusing the electron beam in these aggregates removes the organic matter in these agglomerates, thereby showing much smaller and crystalline primary MXene particles. Table 1 also lists this primary lateral particle size based on high resolution TEM images. It can be concluded from these values that solvent influences the lateral size of MXene particles. The influence of solvent in the ablation process can be understood considering that ablation occurs due to mechanical and thermal shock at the MAX particles. Mechanical forces in a liquid medium are related to viscosity. As seen in Table 1, low viscosity solvents such as methanol, give particles of small lateral average size, while more viscous solvents tend to give in the laser ablation process large average lateral dimensions even in the range



Scheme 1. Pictorial illustration of the preparation of Ti₃C₂ dots by liquid-phase laser ablation.

 $\label{eq:table 1} \textbf{List of } Ti_3C_2 \ dots \ synthesized \ by \ laser \ ablation \ in \ liquid \ phase \ suspension \ of \ Ti_3AlC_2 \ using \ different \ solvents \ and \ relevant \ spectroscopic \ and \ structural \ characterization \ data.$

Solvent	Average particle size (nm)	FT-IR spectroscopy bands $(cm^{-1})^{\dagger}$	Fringe distance (nm) ^a
Metanol	14 ± 8	2950 - 2800 (C-H-) ^a 1260 - 1000 (C- <i>O</i> -) ^b 800 - 500 (Ti- <i>O</i> -) ^c	0.261
n-Propanol	16 ± 7	2950–2800 (C–H-) ^a 1260 - 1000 (C– <i>O</i> -) ^b 800 - 500 (Ti– <i>O</i> -) ^c	0.270
n-Butanol	52 ± 13	2950 - 2800 (C–H-) ^a 1260–1000 (C–O-) ^b 800 - 500 (Ti–O-) ^c ~1600 (Ti–OH) ^d ~720 (–CH ₂ – Rocking band) ^e	0.258
iso-Butanol	53 ± 5	2950–2800 (C–H-) ^a ~1600 (Ti–OH) ^d ~1465 (CH ₂) ^f ~1375 (CH ₃) ^g 1260 - 1000 (C–O-) ^b 800 - 500 (Ti–O-) ^c ~720 (-CH ₂ rocking band) ^e	0.269
Benzyl alcohol	55 ± 2	3020-3000 (C-H-) ^a 1600 (Ti-OH) ^d ~1600; ~1475 (-C=C-) ^h 1260 - 1000 (C-O-) ^b 800 - 500 (Ti-O-) ^c 770-730; 715-685 (monosubstituted aromatic) ⁱ	0.261
Allylic alcohol	4.5 ± 0.5	3600 - 3300 (OH-) ^h 2950 - 2800 (C-H-) ^a 1690-1630 (-C=C- isolated) ^j ~1600 (Ti-OH) ^d 1260 - 1000 (C-O-) ^b 800 - 500 (Ti-O-) ^c	0.269
n-Octanol ^b	27 ± 5	2950 - 2800 (C–H-) ^a ~1600 (Ti–OH) ^d ~1465 (CH ₂) ^f ~1375 (CH ₃) ^g 1260 - 1000 (C–O-) ^b 800 - 500 (Ti–O-) ^c ~720 (-CH ₂ Rocking band) ^e	0.261
2,2,2- Trifluoroethanol	7.2 ± 0.5	2950 - 2800 (C–H-) ^a 1260 - 1000 (C– <i>O</i> -) ^b 800 - 500 (Ti– <i>O</i> -) ^c	0.253
$\underset{d}{\text{Ethanol}} + \text{TBAOH}$	3.14 ± 0.07	2950 - 2800 (C–H-) ^a 1260 - 1000 (C– <i>O</i> -) ^b	0.269

¹ The letters in superscript after the wavenumber and assignment correspond to the bands labelled with the same letter in the corresponding FT-IR spectra shown either in Fig. 2 or Fig. S2 in the supporting information.

of 50 nm. Thus, methanol and n-butanol have a viscosity of 0.54 and 2.63 cP, respectively, and the $\rm Ti_3C_2$ dots resulting in these two solvents have average lateral sizes of 14 ± 8 and 52 ± 13 nm, respectively [15]. While viscosity can influence mechanical forces, the thermal stress caused also by the laser pulse on the MAX can be related to thermal conductivity, heat capacity and boiling point. Generally, viscosity and thermal parameters in solvents are also correlated. Thus, physical solvent parameters exerts are remarkable physical in the laser ablation process due to several effects, as observed in Table 1.

Installment on the MXene surface of terminal groups derived from the solvent in which the laser ablation process was carried out was

clearly revealed in most of the cases by FT-IR spectroscopy. Table 1 lists for each sample the most relevant IR vibration peaks. While in some cases, like in the cases of methanol and trifluoroethanol, the IR absorption bands of the corresponding Ti₃C₂ samples were very weak and inconclusive, in accordance of the carbon chain length and surface termination, the intensity of the IR spectra, gradually increased as the alkyl chain length becomes longer, this tendency being clearly illustrated in the series methanol, ethanol, *n*-propanol, and *n*-butanol. Fig. 2 shows the FT-IR spectra of Ti₃C₂(n-BuOH) and Ti₃C₂(i-BuOH) together with the spectra of the corresponding alcohols, showing convincingly the installment on the sample of alkoxy groups on the surface of the Ti₃C₂. Comparison with the FT-IR spectra of pure *n*- and *i*-butanol shows the absence of -O-H vibration band in the 3500-3200 cm⁻¹ and 1260-1000 cm⁻¹ zones and some notable shifts in the position of the characteristic C-H vibrations. The possibility that these FT-IR spectra correspond to organic by-products formed in the laser irradiation of *n*- or i-butanol was considered and dismissed. Thus, blank controls in the absence of Ti₃AlC₂ were performed for pure *n*- or *i*-butanol solutions, whereby no residue was obtained This comparison and blank control clearly show that the FT-IR spectra of Ti₃C₂(*n*-BuOH) and Ti₃C₂(*i*-BuOH) do not correspond to *n*- or *i*-BuOH or products derived therefrom.

Fig. S2 in the Supporting information shows a collection of FTIR spectra for other samples of the series prepared in the present study. In most of the cases these spectra provide conclusive evidence that the MXene sample contains after the ablation attached to the solid particles the alkoxy chains introduced by the solvent. It should be noted that in the laser etching in benzyl and allylic alcohols, the process results in some oligo-/polymerization of these alcohols and, therefore, even after exhaustive washing and careful removal of the organic solvents, the FT-IR spectra contained spurious peaks of these organic oligomers. However, blank controls in the absence of MAX precursor indicate that these oligomers are not formed for other alcohols. Overall, the FT-IR pectroscopic study is in agreement with the TEM measurements that revealed the presence of organic polymeric matter for Ti₃C₂(BnOH) and Ti₃C₂(CH₂—CHCH₂OH)), but no in the other cases.

At this point, preliminary photocatalytic measurements for hydrogen generation in the presence of methanol showed differences on the performance of these samples, the most active materials being Ti₃C₂(n- $C_8H_{17}OH$), $Ti_3C_2(CF_3CH_2OH)$ and $Ti_3C_2(EtOH + TBAOH)$. Thus, although the previous FT-IR spectra have shown the general applicability of liquid phase laser ablation as physical etching method to form MXene dots from the MAX phase without the use of chemical etchants, while at the same time introducing a variety of alkoxy units on the MXene surface, further characterization was carried out only for these three most active samples. Regarding the reason of the higher activity of these three samples, it is worth noting that according to Table 1, Ti₃C₂(CF₃CH₂OH) and Ti₃C₂(EtOH + TBAOH) are the MXene dots with the smallest lateral size, thereby suggesting a relationship between small size and higher photocatalytic activity. In the case of Ti₃C₂(*n*-C₈H₁₇OH), the lateral size was notably higher, but this sample corresponds to the longest alkyl chain and, therefore, it is likely to be the most hydrophobic surface.

AFM frontal images of these three samples provide a broad field view of the particle size distribution. Fig. 3 shows representative AFM images and vertical profile measurements for these three most active samples. Data on the average thickness of the particle size determined by AFM for these three samples are given in Table 1 as footnotes. These AFM measurements provide an indication about the number of MXene layers in the stacking. Particularly in the case of $Ti_3C_2(CF_3CH_2OH)$, the dots are mono- or bilayers, while in the case of $Ti_3C_2(EtOH + TBAOH)$, the sample has few layers with an average of 3 or 4. Of the three MXene dots, $Ti_3C_2(n-C_8H_{17}OH)$ is the sample with the largest number of monolayers in average. Therefore, it is evident that there is a correlation between viscosity of the liquid medium in which the ablation takes place and the resulting dimensions and average number of layers of the MXene particles. It should be commented at this point that since surface

^a Determined by high resolution TEM.

 $[^]b\,$ Bandgap and average thickness 1.91 eV and 6.5 \pm 0.8 nm.

 $[^]c$ Bandgap and average thickness 1.75 eV and 1.6 \pm 0.1 nm.

 $^{^{}d}\,$ Bandgap and average thickness 1.71 eV and 3.5 \pm 0.3 nm.

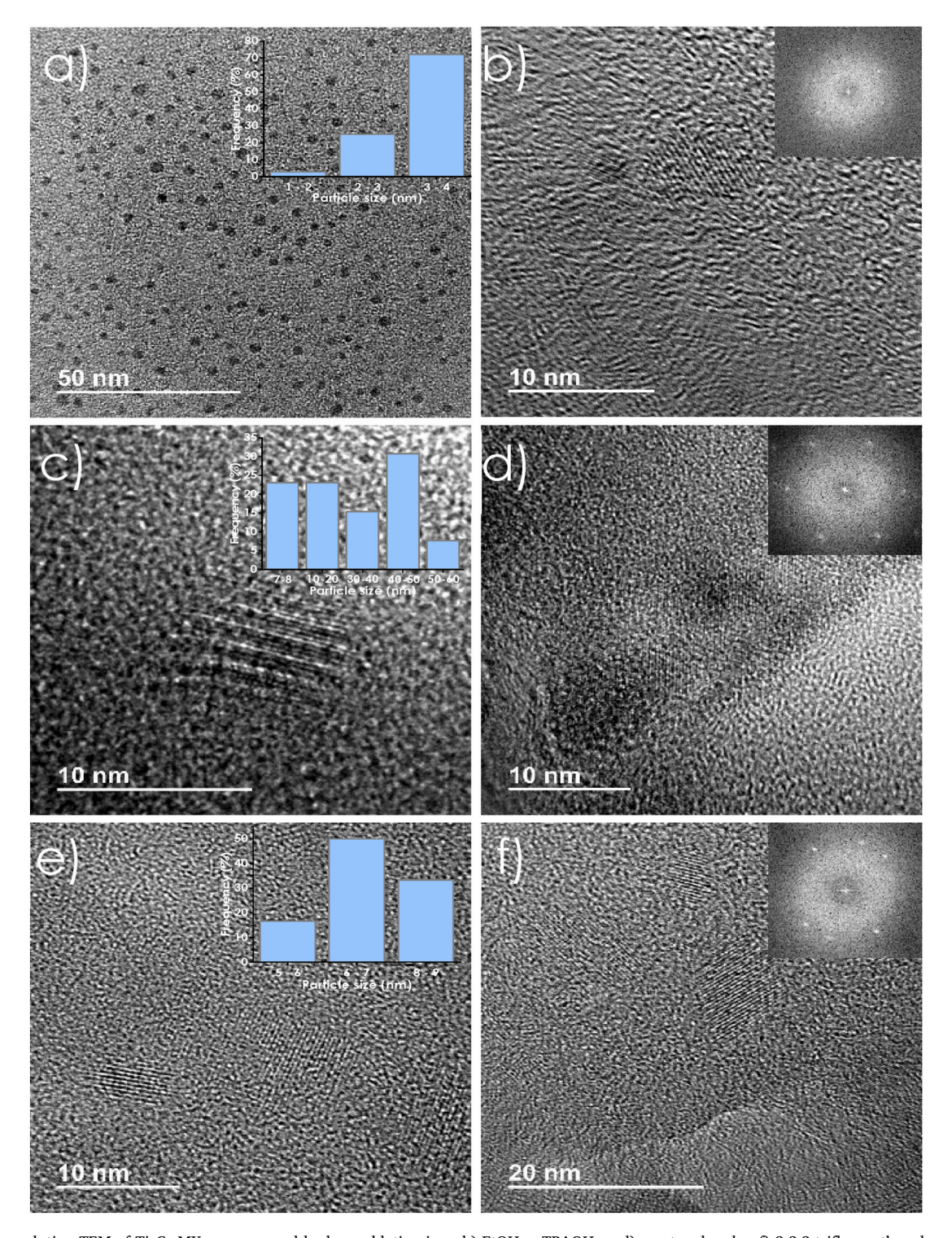


Fig. 1. High-resolution TEM of Ti_3C_2 MXenes prepared by laser ablation in a, b) EtOH + TBAOH, c, d) n-octanol and e, f) 2,2,2-trifluoroethanol suspension. The insets in frames a, c and d show histograms of the lateral particle size distribution, while the insets of images b, d and e correspond to the selected area electron diffraction confirming the crystallinity of the MXene dots.

functionalization of ${\rm Ti_3C_2}(n\text{-}C_8H_{17}OH)$ contains a long alkyl chain, the exact number of average layers cannot be determined from the particle thickness with the current data. Nevertheless, from the increment in the interlayer distance reported in the literature as a function of the surface termination in other cases [16], it can be expected a monolayer thickness around 1.1 nm and, therefore, a reasonable average number of stacking MXene sheets for ${\rm Ti_3C_2}(n\text{-}C_8H_{17}OH)$ should be 6.

XPS analyses of the $Ti_3C_2(n\text{-}C_8H_{17}OH)$, $Ti_3C_2(CF_3CH_2OH)$ and

 $\rm Ti_3C_2(EtOH+TBAOH)$ samples revealed the presence of the expected Ti, C and O elements, as well as F and N in the last two samples. Fig. 4 presents the analysis of selected XPS peaks for these samples, while Fig. S3 in supporting information shows additional XPS data. For $\rm Ti_3C_2(\textit{n-}C_8H_{17}OH)$, the Ti2p core level splits into two peaks due to spin-orbit coupling, each of them having components corresponding to Ti–C (460.7 eV for Ti2p_{1/2}) and Ti–O (464.2 eV for Ti2p_{1/2}). The XPS Ti2p peak of Ti₃C₂(EtOH+TBAOH) exhibits the same components. In

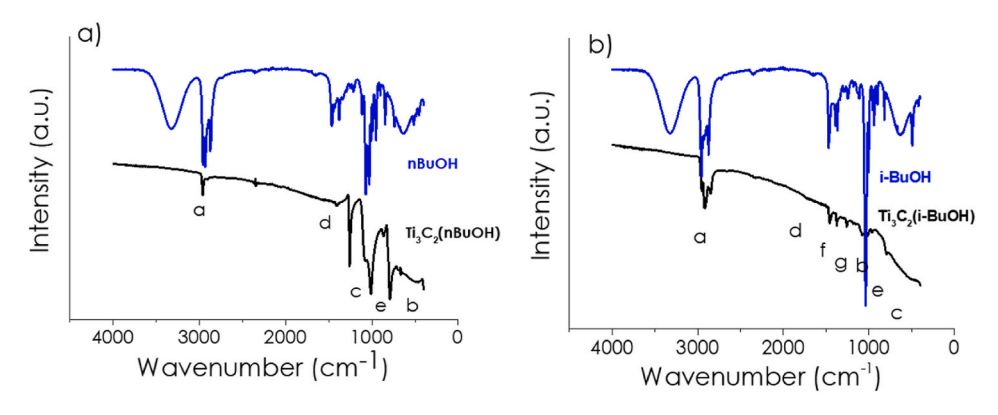


Fig. 2. Comparison of the FT-IR spectra of the solvent and those of the Ti_3C_2 samples prepared in it: a) n-butanol and Ti_3C_2 (BuOH), and b) i-butanol and Ti_3C_2 (i-BuOH). The letters indicate the bands whose wavenumbers are listed in Table 1 in the corresponding column.

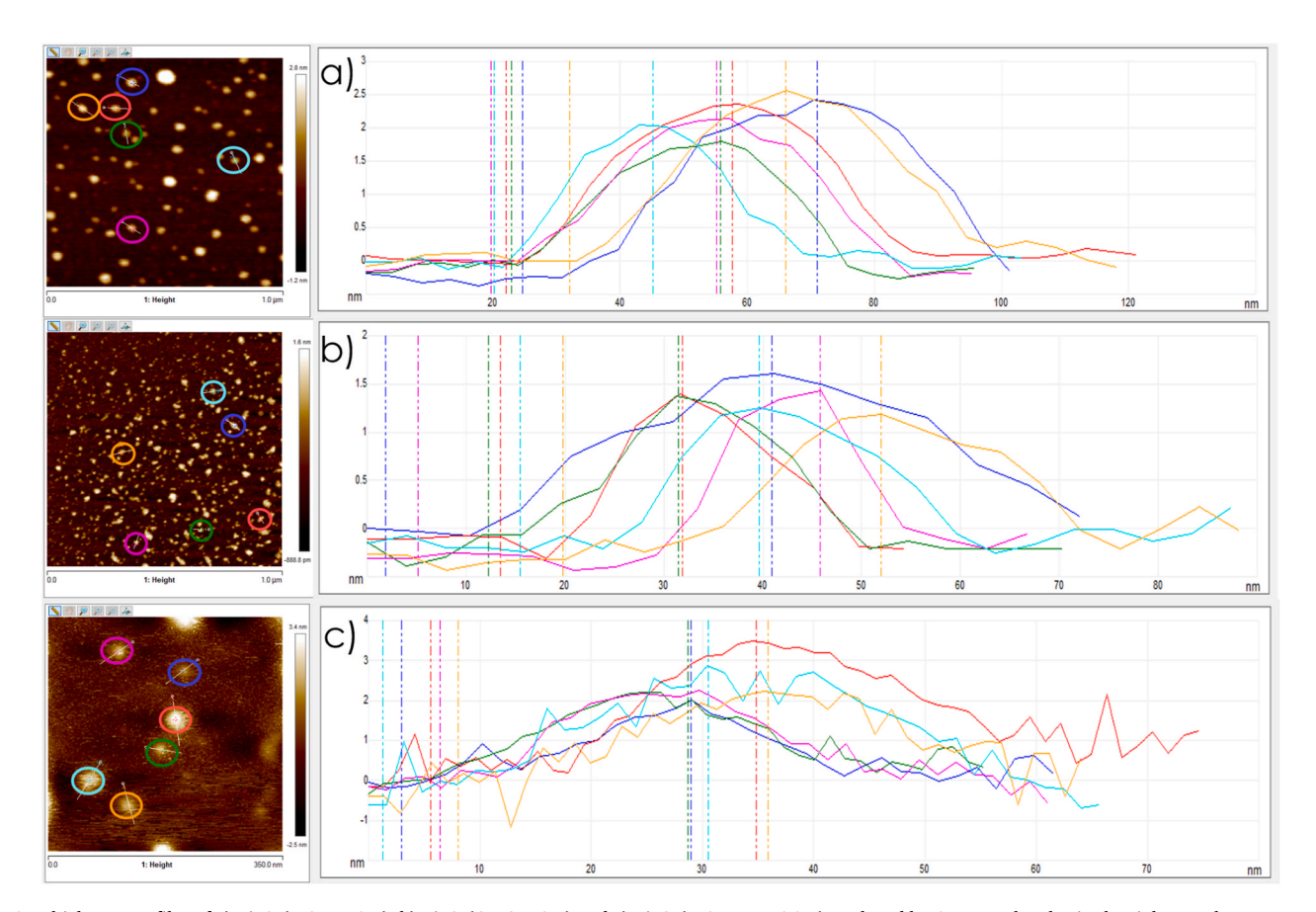


Fig. 3. Thickness profiles of a) $Ti_3C_2(n-C_8H_{17}OH)$, b) $Ti_3C_2(CF_3CH_2OH)$ and c) $Ti_3C_2(EtOH+TBAOH)$ analyzed by AFM. Each color in the right panels correspond to the height of a different nanoparticle of the right panel. (For interpretation of the references to color in this figure legend, the reader is referred to the Web version of this article.)

comparison, Ti2p signal for $Ti_3C_2(CF_3CH_2OH)$ was more complex. The experimental XPS Ti2p peak exhibits three relative maxima at 458.9 eV, 460.2 eV (Ti–C) and 464.22 eV (Ti–O). The new Ti component at 458.9 eV can be attributed to Ti–F. In fact for $Ti_3C_2(CF_3CH_2OH)$ an XPS F1s peak with three individual components at 685.0, 686.6 and 688.3 eV attributable to C–Ti–F, AlFx and Al(OF)x, respectively, was also recorded. These XPS data indicate the generation of HF during the laser ablation in CF_3CH_2OH and it results in the preferent Ti binding with generated F. Also in the case of $Ti_3C_2(EtOH + TBAOH)$, the presence of N was detected in the XPS elemental analyses. The corresponding XPS N1s peak was deconvoluted in two components appearing at 399.8 and 402.3 eV that can be assigned to N atoms bonded to Ti–N and N–H,

respectively.

Regarding analysis of the XPS C1s peak for these three samples, the experimental spectra showed some common traits with components at 284.5 eV and 287.3 eV that can be assigned to C atoms bonded to C and O, respectively. In addition, the XPS C1s for ${\rm Ti}_3{\rm C}_2(n{\rm -}{\rm C}_8{\rm H}_{17}{\rm OH})$ and ${\rm Ti}_3{\rm C}_2({\rm CF}_3{\rm CH}_2{\rm OH})$ presented an additional component at 282.2 eV corresponding to Ti–C, but this component was absent in ${\rm Ti}_3{\rm C}_2({\rm EtOH} + {\rm TBAOH})$. It should be commented that the intensity of the 282.2 eV peak for C–Ti is known to depend on the preparation method of the MXene, being for instance, much lower for materials prepared by the molten salt etching in comparison to those ${\rm Ti}_3{\rm C}_2$ samples prepared using fluorinated etching agents [17]. It has been reported that the XPS C1s peak of MXene

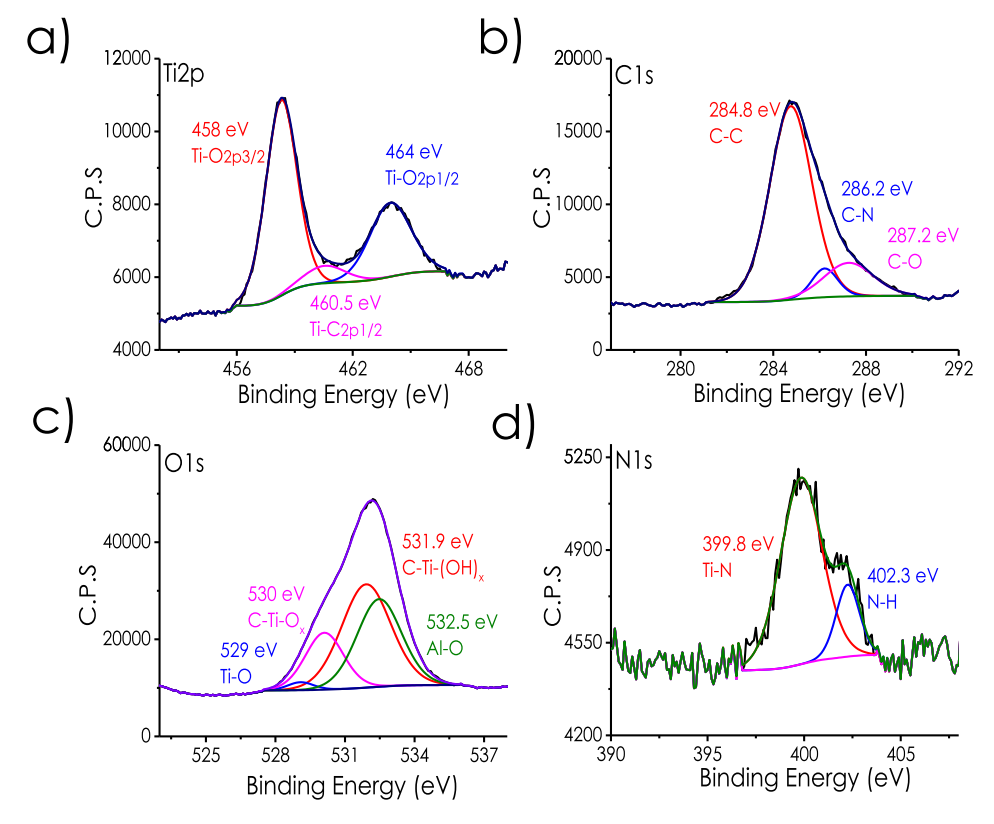


Fig. 4. XPS analysis of Ti₃C₂(EtOH + TBAOH) with high-resolution a) Ti₂p, b) C1s, c) O1s and d) N1s core levels.

dots do not have a separate 282.2 eV peak, but a component at this binding energy value [18]. The same situation seems to be observed here. Although more data are necessary to fully clarify this point regarding the XPS C–Ti component at 282.2 eV, it has to be noted that herein we are dealing with small 0 D MXene particles of a few nm of lateral dimensions in which the relevant proportion of peripheral atoms vs. the *in plane* basal atoms must be considerably higher than in conventional micrometric MXene flakes. In any case, it is worth noting that notable differences in XPS data depending on the preparation procedure have been already noted in MXenes [17].

In addition, the presence of residual Al was also detected in these three samples as a peak with a single component at 74.1 eV matching well with the binding energy of Al–O for $Ti_3C_2(n-C_8H_{17}OH)$ and $Ti_3C_2(EtOH + TBAOH)$ [19] or as a single component appearing at 76.0 eV attributable to Al–F in the $Ti_3C_2(CF_3CH_2OH)$ (Fig. S3) [20].

Summing up the information of XPS it can be concluded that due to the presence of alkyl chains on the surface, the C1s has a negligible C–Ti component at 282.2 eV, but this type of bond is deduced from the analysis of Ti2p core level. Also, Al is detected as Al_2O_3 or as Al–F, but not as in the Ti_3AlC_2 precursor. But, the XPS data is crucial to determine that the ablation in CF_3CH_2OH , generates fluoride that is the species preferentially installed on the $Ti_3C_2(CF_3CH_2OH)$ surface rather than the poor nucleophilic alcohol. It is proposed that this *in situ* generated fluoride species could be an attractive alternative to the current HF etching procedures that employ a large excess of this acid.

The fact that the samples prepared by laser ablation correspond to MXene and not to the MAX precursor is firmly supported by TEM images and selected area electron diffraction of all the MXene dots. In the case of ${\rm Ti}_3{\rm C}_2({\rm EtOH})$, the MXene nature of the sample after laser ablation was double checked by PXRD. Fig. S4 shows a comparison of the diffraction pattern of ${\rm Ti}_3{\rm AlC}_2$ MAX precursor with that of the ${\rm Ti}_3{\rm C}_2({\rm EtOH})$ after laser ablation.

2.2. Photocatalytic overall water splitting

Regarding the photochemical properties of the Ti₃C₂ dots, one important property is the optical absorption spectrum of the samples, since it gives direct information on the electron excitation wavelength and bandgap energy of the material. The UV-Vis absorption spectra for the Ti₃C₂ dots show an almost neutral absorption throughout the UV-Vis spectral range with an abrupt absorption in the deep UV region, below 250 nm, the onset appearing at about 300 nm in the case of Ti₃C₂(n-C₈H₁₇OH). For Ti₃C₂(CF₃CH₂OH), a weak and broad plasmon band with an absorption maximum at 500 nm was recorded. Fig. 5 shows some illustrative UV-Vis absorption spectra, while Fig. S5 in supporting information presents a more complete set of diffuse-reflectance UV-Vis absorption spectra for the other Ti₃C₂ dots. As a general trend, a red-shift in the onset was observed with the increase of the alkyl chain length. In the case of Ti₃C₂(BnOH) and Ti₃C₂(CH₂=CHCH₂OH) similar optical spectra with two defined shoulders in the UV region with relative absorption maxima at 220 and 270 nm were recorded, but they could

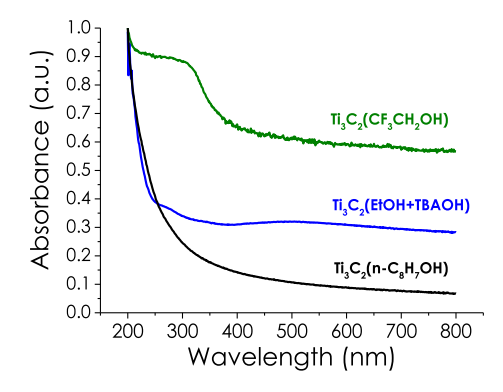


Fig. 5. UV–vis absorption spectra of ${\rm Ti_3C_2}(n\text{-}C_8H_{17}OH)$, ${\rm Ti_3C_2}({\rm CF_3CH_2OH})$ and ${\rm Ti_3C_2}({\rm EtOH}+{\rm TBAOH})$.

correspond to the organic polymers present in these samples. Also, remarkably different was the case of ${\rm Ti_3C_2(CF_3CH_2OH)}$ that exhibits an absorption band at 290 nm and onset at 390 nm. It is proposed that these significant changes in the absorption spectra derive from differences in the surface terminal groups and on the lateral size of the MXene particles. In any case, the results show the possibility to have a certain control on the optoelectronic properties of the resulting MXene by appropriate selection of the laser ablation media and conditions.

MXenes have been reported among the best electrocatalysts for hydrogen evolution reaction and oxygen reduction reaction [21]. Besides as electrocatalysts, MXenes are increasingly used as photocatalysts, either acting as co-catalysts in combination with organic dye photosensitizers or even with intrinsic photocatalytic activities [22]. We have previously shown that MXene dots exhibit photocatalytic activity for hydrogen evolution and CO₂ reduction [18,23], there being of interest to extend further the knowledge on the photocatalytic activity of these materials. Herein, we provide experimental information about the influence of surface functional groups on the photocatalytic activity. It is well known from DFT calculations that the nature of the surface functional groups play an important role on the electronic properties of MXenes, including electrical conductivity and the shift from conductive to semiconducting materials [24]. In particular, photocatalytic activity of MXenes depend on the surface terminal groups due a combination of factors including: i) variation of bandgap and, therefore, optical absorption and light harvesting; ii) charge separation efficiency due to surface sites acting as charge carrier trap sites, and iii) charge carrier migration length. All these photophysical parameters, as well as the presence of vacancies and gas evolution sites depend on the nature of surface terminations. Therefore, it is important to determine for MXene dots prepared under analogous conditions, in which extent the surface terminal groups influence the photochemical properties. Due to its current importance, the present study is focused on the photocatalytic overall water splitting and H2 evolution.

Preliminary studies irradiating with the full UV–Vis output of a 150 W Xe lamp showed that, although these MXene dots were able to promote overall photocatalytic water splitting, their activity was low in most of the cases. The three most active samples were, as indicated previously, ${\rm Ti}_3{\rm C}_2({\rm r-C}_8{\rm H}_{17}{\rm OH})$, ${\rm Ti}_3{\rm C}_2({\rm CF}_3{\rm CH}_2{\rm OH})$ and ${\rm Ti}_3{\rm C}_2({\rm EtOH} + {\rm TBAOH})$ that were selected for further studies. Fig. 6 presents the temporal profile of ${\rm H}_2$ and ${\rm O}_2$ evolution upon irradiation using these three samples as photocatalysts. The relative activity follows the order

 ${\rm Ti}_3{\rm C}_2({\rm EtOH} + {\rm TBAOH}) > {\rm Ti}_3{\rm C}_2({\rm CF}_3{\rm CH}_2{\rm OH}) > {\rm Ti}_3{\rm C}_2(n{\rm -C}_8{\rm H}_{17}{\rm OH}).$ Notable values of H₂ evolution were obtained, particularly for ${\rm Ti}_3{\rm C}_2({\rm EtOH} + {\rm TBAOH})$ that reached in overall water splitting for the fresh material a H₂ productivity of 5 mmol g⁻¹ in 24 h. Control experiments showed that the photocatalytic activity of ${\rm Ti}_3{\rm C}_2({\rm EtOH})$ or ${\rm Ti}_3{\rm C}_2({\rm TBAOH})$ was considerably lower and, therefore, the combination of TBAOH during the laser ablation in ethanol is crucial for the observed performance. TBAOH has been reported in the etching procedure as a way to install –OH groups on the ${\rm Ti}_3{\rm C}_2$ surface [25,26] and we have found here by XPS analyses the presence also N-alkyl groups, while the low boiling point and viscosity of ${\rm CH}_3{\rm CH}_2{\rm OH}$ is favorable for producing dots of small lateral size.

To put the results shown in Fig. 6 into a broader context, Table S1 summarizes data reported in the literature for other Ti photocatalysts. Although comparison with reported data from other laboratories should be made with caution, Table S1 shows that the performance of $\rm Ti_3C_2(EtOH + TBAOH)$ compares favorable with that other other Ti photocatalysts. It should be noted that $\rm Ti_3C_2(EtOH + TBAOH)$ is a single component photocatalyst and does not contain noble or semiprecious metal nanoparticles, such as Pt, Au or Ag.

Having established the role of the surface terminal groups on the photocatalytic activity, one important part of the study was to determine MXene stability under the photocatalytic conditions. For the three samples, a considerable degree of deactivation upon reuse was observed. These data are presented in Fig. S6. In the case of $\rm Ti_3C_2(EtOH+TBAOH)$ the photocatalytic activity decreased from 5 mmol g $^{-1}$ in 24 h irradiation for the fresh sample to 0.8 mmol g $^{-1}$ for the same time in the third

To understand the origin of this deactivation upon reuse, the three-times used $\rm Ti_3C_2(EtOH~+~TBAOH)$ dots were characterized by TEM, AFM and XPS. AFM images show the occurrence of particle aggregation during the photocatalytic process resulting in larger and thicker particles. TEM images show a considerable degree of amorphization of the particles that have lost their crystallinity in a large extent. As an example, Fig. S7 shows selected images of the used samples showing the notable crystallinity loss, while Fig. S8 shows AFM measurements reporting agglomeration of MXene dots during the photocatalytic reaction and Fig. S9 presents the XPS of the used photocatalysts.

It is known that MXenes have tendency to undergo oxidative degradation [27]. Although $Ti_3C_2T_x$ is among the most stable MXenes [28,29], it can undergo oxidation when suspended in water [30].

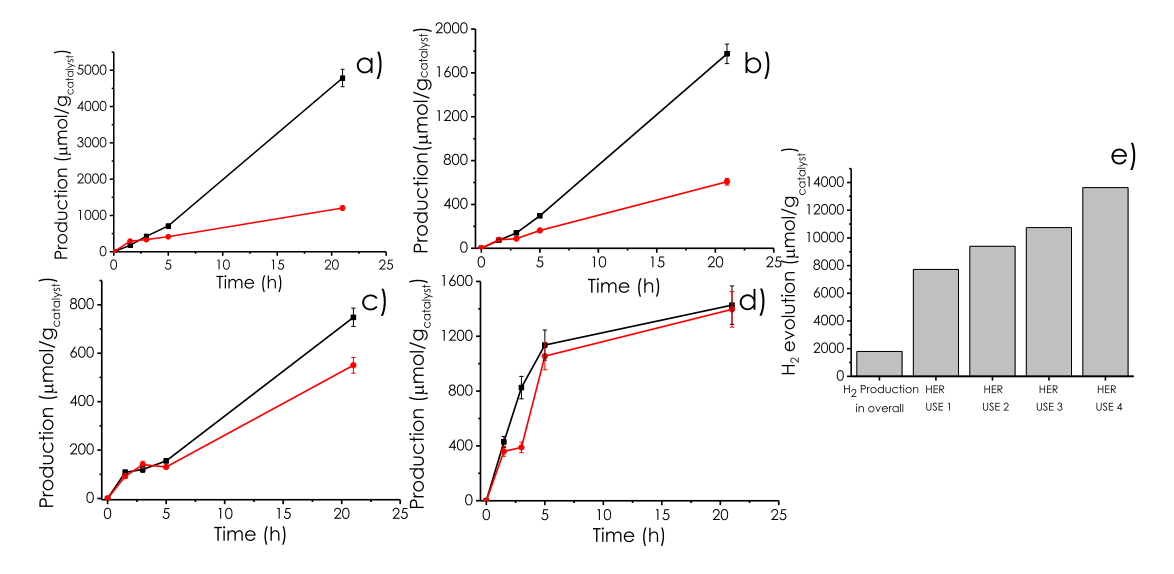


Fig. 6. 1) H_2 and 2) O_2 production using a) $Ti_3C_2(EtOH + TBAOH)$, b) $Ti_3C_2(CF_3CH_2OH)$, c) $Ti_3C_2(n-C_8H_{17}OH)$, and d) $Ti_3C_2(TBAOH + H_2O)$ as photocatalysts in water-splitting reaction. Irradiation conditions Full output of a 150 W Xe lamp through quartz, room temperature under stirring, 1 mg of photocatalyst, 10 ml of distilled water; e) Reusability test of H_2 production reaction using $Ti_3C_2(CF_3CH_2OH)$ as photocatalyst under UV–Visible irradiation using methanol as electron donor and comparing with overall water splitting reaction results after 24 h.

Therefore, it is likely that photoinduced charge separation with the generation of holes could produce self-oxidation of Ti₃C₂T_x, particularly when sacrificial electron donors are not present. If this were the case, then, photoirradiation in the presence of electron donors could result in an increase of the photochemical stability of MXene as consequence of the quenching of the photogenerated holes causing self-oxidation. To test this hypothesis on the occurrence of MXene degradation due to self-oxidation, while at the same time follow the alteration of the surface termination, photocatalytic hydrogen generation using Ti₃C₂(CF₃. CH₂OH) dots was carried out in the presence of methanol. The results are presented in Fig. 6 e). Besides an expected higher increase in H2 evolution under these conditions going from 1800 to 7800 μmol_{H2} $g_{catalyst}^{-1}$, the most surprising, unexpected fact was the observation of a gradual increase in the amount of evolved H2 upon reuse. Therefore, the presence of a sacrificial electron donor not only increases considerably the photocatalytic stability of Ti₃C₂(CF₃CH₂OH) dots as photocatalyst, but also makes the material gradually more active upon reuse. TEM analysis of the Ti₃C₂(CF₃CH₂OH) after the four times use revealed as shown in Fig. S10 that the crystallinity of the MXene has been maintained under these conditions, without amorphization of the MXene dots. This performance and the photocatalytic results in the presence of methanol lend support to self-oxidation by photogenerated holes as the most reasonable cause of Ti₃C₂(CF₃CH₂OH) dots instability in the overall water splitting photocatalytic irradiation resulting in the gradual conversion into amorphous TiO2.

Regarding the increase in the photocatalytic hydrogen evolution rate upon reuse of $Ti_3C_2(CF_3CH_2OH)$ dots, two possibilities were considered. The first one would the partial self-oxidation of $Ti_3C_2(CF_3CH_2OH)$ forming an efficient heterojunction between the photogenerated TiO_2 and $Ti_3C_2(CF_3CH_2OH)$ dots. However, this type of $Ti_3C_2T_2/TiO_2$ heterojunctions have been already reported in the literature, observing only a moderate increase in the photocatalytic activity [31,32]. However this possibility seems unlikely in the present case due to the fact that the crystallinity of $Ti_3C_2(CF_3CH_2OH)$ is preserved in the process, without observing TiO_2 formation as determined by TEM.

An alternative explanation in line with the present results in which each Ti₃C₂ dot sample exhibits different photocatalytic activity depending on the surface groups would be the gradual spontaneous upgrading of the surface termination composition to result in the optimal photocatalytic performance. Evidence in support of this second alternative was obtained by XPS analysis comparing the percentage of F and O atoms on the surface of fresh Ti₃C₂(CF₃CH₂OH) dot that were 13.6 and 14.2 at.%, respectively, with that of the four times used sample of the experiment indicated in Fig. 6e. As shown in Fig. S11, XPS analysis of the four times used Ti₃C₂(CF₃CH₂OH) dot sample revealed that the F atoms present in the fresh Ti₃C₂(CF₃CH₂OH) dots (Fig. S3) are completely lost in the photocatalytically most active four-times used Ti₃C₂(CF₃CH₂OH) sample, while the O content increased up to 55.4 at.% of the surface atoms. This variation in the analysis of the surface termination indicates that surface F atoms are replaced by oxygenated groups during operation of the photocatalytic reaction. This proposal will agree with the maintenance of MXene dot crystallinity and with the loss of F atoms by XPS. Theoretical studies have predicted that semiconducting properties of MXenes should be strongly dependent on the nature of the surface termination and our results would imply that the photocatalytic activity of fluorinated Ti₃C₂(CF₃CH₂OH) would be lower than the oxygenated MXene dot [24].

To provide further support to this claim of variation of the surface terminal groups during the photocatalytic experiments, a similar XPS analysis of the atomic composition of the surface groups was performed for the $\rm Ti_3C_2(EtOH+TBAOH)$ sample, comparing the fresh and the used samples. As shown in Fig. S9, it was determined that the O1s core level of $\rm Ti_3C_2(EtOH+TBAOH)$ contains a component for O in adsorbed $\rm H_2O$ of 8.2 at.%, while the O atoms attached to $\rm Ti_3C_2$ account for 32.8 at.%. After its use as photocatalyst, O atomic percentage in the surface increased to 38.3 at.%, thus, showing again an increase in O content.

3. Conclusions

It has been shown that liquid phase laser ablation is a suitable physical etching technique that, simultaneously with chemical-free Al etching of $\rm Ti_3AlC_2$ and formation of $\rm Ti_3C_2T_x$ nanoparticles of small dimensions and thickness, installs on the surface a variety of alkoxy groups. Average particle size and number of stacking layers were found to depend on the viscosity of the solvent and they can vary from a few nanometers to tens of nanometers, thus, offering a notable control on the lateral size by wise selection of the solvent. In the case of trifluoroethanol, laser induced HF generation efficiently introduces on the surface F atoms, but avoiding the need of using concentrated fluorinated reagents. It is reasonable to assume that this technique can also serve to introduce other functional groups and will be general for other MXenes. Particularly, tetrabutylammonium can be used to introduce nitrogenated groups on the surface.

The resulting Ti₃C₂T_x nanoparticles exhibit photocatalytic activity for overall water splitting, the performance depending on the nature of the alkoxy group. It was found that the Ti₃C₂T_x dots were not stable during the operation of the photocatalytic process, undergoing a gradual oxidative degradation to an amorphous TiO₂ material. Considering that MXene dots are stable in the photocatalytic hydrogen generation when methanol as sacrificial electron donor is present, the most likely cause of photocatalytic instability appears to be self-oxidation by photogenerated holes. The increase in photocatalytic activity for hydrogen generation in the presence of methanol upon reuse, accompanied by changes in the nature of the surface groups indicates that there should be optimum terminations to achieve the highest efficiency and opens the door for S-scheme heterojunctions in which MXene would act as reduction photocatalyst accompanied by an oxidation photocatalyst. Further work is in progress to expand the present chemical-free synthetic procedure for the preparation of MXene nanoparticles with other surface groups and for other applications.

4. Experimental section

4.1. Liquid-phase laser ablation

10~mg of Ti_3AlC_2 (Chemazone) were suspended in 4 mL of the corresponding alcohol and placed in a quartz cuvette capped with a septum. The suspensions were deaerated by flushing Ar with a needle for at least 15 min before starting the ablation. The suspension was magnetically stirred with a magnetic bar throughout the process. The suspension was irradiated with the second harmonic (532 nm) of a pulsed Nd-YAG laser (7 ns pulse width, 10 pulses \times s $^{-1}$, 35 mJ \times pulse $^{-1}$) for 3 h. After this time, the solids were decanted and the supernatant was collected. The solvent was removed under reduced pressure.

4.2. Characterization techniques

Transmission electron microscopy (TEM) micrographs of the MXene dots were acquired with a JEOL JEM 2100F electron microscopy operating as accelerating voltage at a potential of 200 kV. The samples were well dispersed in methanol using an ultrasound bath and, then, a microdrop of this suspension was deposited on a conductive carboncoated holey Ni grid holder. The solvent was allowed evaporating at ambient temperature, before introducing the sample in the microscope chamber.

AFM images and thickness measurements were carried out in the tap mode using a Bruker Multimode 8 Nanoscope instrument with vertical and horizontal resolution of 0.3 and 5 nm, respectively. A drop of MXene dots in aqueous suspension was deposited onto atomically flat mica wafer and water allowed to evaporate at ambient temperature before measurements.

Attenuated total reflectance Fourier transformed IR (ATR-FTIR) spectra were recorded using a Bruker Tensor 27 spectrophotometer

having a diamond ATR accessory measuring from 4000 to 400 cm $^{-1}$ with a resolution of 4 cm $^{-1}$ and averaging eight spectra. AFM, UV–Vis spectra were recorded in aqueous suspension using a Cary 100 spectrophotometer. XPS analyses were acquired on a SPECS instrument using as detector a Phoibos 1509MCD setup. Excitation source consisted on a non-monochromatic X-ray emitter (Al and Mg) operating at 200 W. The operation pressure of the systems was 1×10^{-9} mbar. The signal intensity of the peaks was determined from the area of the corresponding peaks after background subtraction using the nonlinear Shirley function and corrected by the relative response factor of each element for XPS. The binding energy of the peaks were calibrated using 284.6 eV as the value for the maximum of the C1s peak.

4.3. Photocatalytic experiments

The photocatalyst was dispersed in 20 mL of Milli-Q $\rm H_2O$ or a mixture of Milli-Q $\rm H_2O$:MeOH (4:1) for the hydrogen evolution experiments and the suspension was introduced in a quartz reactor (51 mL). The system was purged with Ar and sonicated twice for 20 min to ensure a good solid dispersion of the MXene dot. The suspension was irradiated under continuous magnetic stirring with a Xe lamp (150 W). The gas production was analyzed at different times by analysis of the head space mixture using an Agilent490 MicroGC system (5 Å molecular sieves column using Ar as carrier gas).

CRediT authorship contribution statement

Rubén Ramírez-Grau: Investigation. María Cabrero-Antonino: Investigation. Francis Rey Cortes: Investigation. Gladys Mínguez-Vega: Investigation. Matthew G. Quesne: Investigation. C. Richard A. Catlow: Investigation. Jose A. Mata: Investigation, Conceptualization. Hermenegildo García: Writing – review & editing, Writing – original draft, Conceptualization. Ana Primo: Writing – review & editing, Writing – original draft, Conceptualization.

Declaration of competing interest

The authors declare that they do not incur in any conflict of interests.

Acknowledgements

Financial support by the Spanish Ministry of Science and Innovation (CEX-2021-001230-S and PDI2021-0126071-OB-CO21 and PDI2021-0126071-OB-CO22 funded by MCIN/AEI/10.13039/501100011033), Generalitat Valenciana (Prometeo 2021/038 and Advanced Materials programme Graphica MFA/2022/023 with funding from European Union NextGenerationEU PRTR-C17.I1) and European Commission (ERC Discovery) are gratefully acknowledged.

Appendix A. Supplementary data

Supplementary data to this article can be found online at $\frac{https:}{doi.}$ org/10.1016/j.ijhydene.2025.152298.

References

- [1] Cao M-S, Cai Y-Z, He P, Shu J-C, Cao W-Q, Yuan J. 2D MXenes: electromagnetic property for microwave absorption and electromagnetic interference shielding. Chem Eng J 2019;359:1265–302.
- [2] Bai S, Yang M, Jiang J, He X, Zou J, Xiong Z, Liao G, Liu S. Recent advances of MXenes as electrocatalysts for hydrogen evolution reaction. npj 2D Mater Applications 2021;5:78.
- [3] Shuck CE, Ventura-Martinez K, Goad A, Uzun S, Shekhirev M, Gogotsi Y. Safe synthesis of MAX and MXene: guidelines to reduce risk during synthesis. ACS Chem Health Safety 2021;28:326–38.

- [4] Siddique S, Waheed A, Iftikhar M, Mehran MT, Zarif MZ, Arafat HA, Hussain S, Shahzad F. Fluorine-free MXenes via molten salt Lewis acidic etching: applications, challenges, and future outlook. Prog Mater Sci 2023;101183.
- [5] Natu V, Barsoum MW. MXene surface terminations: a perspective. J Phys Chem C 2023;127:20197–206.
- [6] Tang M, Li J, Wang Y, Han W, Xu S, Lu M, Zhang W, Li H. Surface terminations of MXene: synthesis, characterization, and properties. Symmetry 2022;14:2232.
- [7] Khanal R, Irle S. Effect of surface functional groups on MXene conductivity. J Chem Phys 2023;158:194701.
- [8] Zhang N, Hong Y, Yazdanparast S, Zaeem MA. Superior structural, elastic and electronic properties of 2D titanium nitride MXenes over carbide MXenes: a comprehensive first principles study. 2D Mater 2018;5:045004.
- [9] Mansur HS. Quantum dots and nanocomposites. Wiley Interdiscip Rev Nanomed Nanobiotechnol 2010;2(2):113–29.
- [10] Christian P, Von der Kammer F, Baalousha M, Hofmann T. Nanoparticles: structure, properties, preparation and behaviour in environmental media. Ecotoxicology 2008;17:326–43.
- [11] Tang Y, Yang C, Xu X, Kang Y, Henzie J, Que W, Yamauchi Y. MXene nanoarchitectonics: defect-engineered 2D MXenes towards enhanced electrochemical water splitting. Adv Energy Mater 2022;12:2103867.
- [12] Ramalingam G, Kathirgamanathan P, Ravi G, Elangovan T, Manivannan N, Kasinathan K. Quantum confinement effect of 2D nanomaterials. In: Quantum dotsfundamental and applications. IntechOpen; 2020.
- [13] Adibah NA, Zaine SA, Shukur MFA. Synthesis of Ti3C2 mxene through in situ hf and direct hf etching procedures as electrolyte fillers in dye-sensitized solar cell. Mater Sci Forum 2021;1023:15–20. Trans Tech Publ.
- [14] Wang H, Zhang J, Wu Y, Huang H, Li G, Zhang X, Wang Z. Surface modified MXene Ti3C2 multilayers by aryl diazonium salts leading to large-scale delamination. Appl Surf Sci 2016;384:287–93.
- [15] Birch F, Schairer JF, Spicer HC. Handbook of physical constants. Geological Society of America; 1942.
- [16] Yuen ACY, Chen TBY, Lin B, Yang W, Kabir II, Cordeiro IMDC, Whitten AE, Mata J, Yu B, Lu H-D. Study of structure morphology and layer thickness of Ti3C2 MXene with small-Angle neutron scattering (SANS). Composit C 2021;5:100155.
- [17] Natu V, Benchakar M, Canaff C, Habrioux A, Celerier S, Barsoum MW. A critical analysis of the X-ray photoelectron spectra of Ti3C2Tz MXenes. Matter 2021;4: 1224–51.
- [18] Ramírez-Grau R, Cabrero-Antonino M, García H, Primo A. MXene dots as photocatalysts for CO2 hydrogenation. Appl Catal B 2024;341:123316.
- [19] Kloprogge JT, Duong LV, Wood BJ, Frost RL. XPS study of the major minerals in bauxite: gibbsite, bayerite and (pseudo-) boehmite. J Coll interface Sci 2006;296: 572–6.
- [20] Makarowicz A, Bailey CL, Weiher N, Kemnitz E, Schroeder SL, Mukhopadhyay S, Wander A, Searle BG, Harrison NM. Electronic structure of lewis acid sites on high surface area aluminium fluorides: a combined XPS and ab initio investigation. Phys Chem Chem Phys 2009:11(27):5664–73.
- [21] Sajid IH, Iqbal MZ, Rizwan S. Recent advances in the role of MXene based hybrid architectures as electrocatalysts for water splitting. RSC Adv 2024;14:6823–47.
- [22] Grau RR, Lewandowska-Andralojc A, Primo A, García H. Enhancement of the photocatalytic hydrogen production with the exfoliation degree of Nb₂C cocatalyst. Int J Hydrogen Energy 2023;48:20314–23.
- [23] Ramírez R, Melillo A, Osella S, Asiri AM, Garcia H, Primo A. Green, HF-Free synthesis of MXene quantum dots and their photocatalytic activity for hydrogen evolution. Small Methods 2023;7:2300063.
- [24] Ibragimova R, Erhart P, Rinke P, Komsa H-P. Surface functionalization of 2D MXenes: trends in distribution, composition, and electronic properties. J Phys Chem Lett 2021;12:2377–84.
- [25] Liu L, Orbay M, Luo S, Duluard S, Shao H, Harmel J, Rozier P, Taberna P-L, Simon P. Exfoliation and delamination of Ti₃C₂T_x MXene prepared via molten salt etching route. ACS Nano 2021;16:111–8.
- [26] Xu J, Peng T, Zhang Q, Zheng H, Yu H, Shi S. Intercalation effects on the electrochemical properties of ${\rm Ti_3C_2T_x}$ MXene nanosheets for high-performance supercapacitors. ACS Appl Nano Mater 2022;5:8794–803.
- [27] Zhang CJ, Pinilla S, McEvoy N, Cullen CP, Anasori B, Long E, Park S-H, Seral-Ascaso A, Shmeliov A, Krishnan D. Oxidation stability of colloidal two-dimensional titanium carbides (MXenes). Chem Mater 2017;29(11):4848–56.
- [28] Enyashin A, Ivanovskii A. Atomic structure, comparative stability and electronic properties of hydroxylated Ti₂C and Ti3C₂ nanotubes. Comput Theor Chem 2012; 989:27–32.
- [29] Rozmysłowska A, Wojciechowski T, Ziemkowska W, Chlubny L, Olszyna A, Poźniak S, Tomkiewicz K, Jastrzębska A. Colloidal properties and stability of 2D Ti₃C₂ and Ti₂C MXenes in water. Int J Electrochem Sci 2018;13(11):10837–47.
- [30] Tan J, Fan B, Zhang P, Wei Y, Soomro RA, Zhao X, Kumar J, Qiao N, Xu B. Ultralong stability of Ti₃C₂T_x-MXene dispersion through synergistic regulation of storage environment and defect capping with Tris-HCl buffering. Small Methods 2024;2301689.
- [31] Qiang W, Qu X, Chen C, Zhang L, Sun D. Ti3C2 MXene derived (001) TiO₂/Ti₃C₂ heterojunctions for enhanced visible-light photocatalytic degradation of tetracycline. Mater Today Commun 2022;33:104216.
- [32] Xu Y, Wang S, Yang J, Han B, Nie R, Wang J, Wang J, Jing H. In-situ grown nanocrystal TiO₂ on 2D Ti₃C₂ nanosheets for artificial photosynthesis of chemical fuels. Nano Energy 2018;51:442–50.